AIAA JOURNAL
Vol. 40, No. 1, January 2002

Refined Structural Model for Thin- and Thick-Walled Composite Rotor Blades

Sung Nam Jung,* V. T. Nagaraj,† and Inderjit Chopra‡
University of Maryland, College Park, Maryland 20742

A refined structural model based on a mixed force and displacement method is proposed for the analysis of composite rotor blades with elastic couplings. The present formulation allows the modeling of either open-section or closed-section blades of arbitrary section shape, stacking sequence, and end restraint effects. The theory accounts for the effect of elastic couplings, shell wall thickness, section warping, warping restraint, and transverse shear deformations. A semicomplementary energy functional is used to derive, in a variationally consistent manner, the beam force–displacement relations. Bending and torsion related warpings and shear correction factors are obtained in closed form as part of the analysis. The resulting first-order shear deformation theory (Timoshenko) describes the beam kinematics in terms of the axial, flap and lag bending, flap and lag shear, twist, and torsion-warping deformations. The theory is validated against experimental data and other finite element results for graphite–epoxy composite beams of various cross sections such as I sections, box sections, and two-cell airfoils. Good correlation is achieved for all of the test examples. The influence of wall thickness and transverse shear on the static beam response is also investigated. Wall thickness effects are shown to become significant when the thickness-to-depth ratio of the beam reaches around 20%. The slenderness ratio has a significant effect on the transverse shear behavior of the beam, especially for beams with low slenderness ratios. It is also shown that the layup angle has a nonnegligible effect on the transverse shear behavior of the beam.

Nomenclature

a	=	local shell radius of curvature
E_{11}, E_{22}	=	Young's moduli in principal directions
$f_x, f_y, f_z, f_\omega, f_\phi$	=	shear flow components
G_{12}	=	shear modulus
g_y, g_z, g_ω	=	shear correction coefficients
l	=	length of the blade
M_{xx}, M_{ss}, M_{xs}	=	moment resultants for the shell segment
M_y, M_z	=	beam bending moments
M_ω	=	warping moment
m_y, m_z, m_ω	=	applied distributed moments
N	=	axial force of beam
N_{xn}, N_{sn}	=	transverse shear stress resultants for the shell
N_{xx}, N_{ss}, N_{xs}	=	membrane stress resultants for the shell segment
n	=	distributed axial force
q_y, q_z	=	external transverse shear forces
T	=	total torque
T_s	=	St. Venant twisting moment
T_ω	=	Vlasov bimoment
t_s	=	external twisting moment
U, V, W	=	beam displacements
u, v_t, v_n	=	shell displacements
V_y, V_z	=	transverse shear forces
x, s, n	=	coordinate systems for shell wall
x, y, z	=	undeformed beam coordinates
β_y, β_z	=	cross-sectional rotations for the beam
γ_{xn}, γ_{sn}	=	transverse shear strains for the shell
γ_{xy}, γ_{xz}	=	transverse shear strains for the beam
$\varepsilon_{xx}, \varepsilon_{ss}, \gamma_{xs}$	=	membrane strains for the shell
$\kappa_{xx}, \kappa_{ss}, \kappa_{xs}$	=	curvatures
ν_{12}	=	Poisson's ratio in principal plane
ϕ	=	elastic twist deformation

Subscripts

$,s$	=	$\partial/\partial s$
$,x$	=	$\partial/\partial x$

Superscript

T	=	transpose

I. Introduction

DURING the past decade, there has been a phenomenal growth in research activities to develop a methodology to analyze composite tailored rotor blades. These range from simple analytical models to detailed finite element methods. These studies have led to a better understanding of the structural behavior of composite rotor blades and to the importance of nonclassical effects such as out-of-plane warping, warping restraint, and transverse shear on the behavior of composite blades. Jung et al.[1] made an assessment of the current techniques of modeling composite rotor blades and identified, among others, the need for a comprehensive general composite blade analysis that includes such features as elastic couplings, or the variation of stress across shell wall thickness that will be applicable to beams having open or closed multicell generic cross sections. Such a model should also be capable of modeling cross-sectional warping due to bending and torsion.

Composite rotor blades are, in general, built-up structures made of different materials for the skin and spar and may have honeycomb/structural foam fillers for maintaining the airfoil shape, along with leading-edge erosion caps, a provision for antiicing, and balance weights. Main rotor blades are normally of closed single- or multicelled cross sections and are thin walled, except near the root where they become thick walled. Because of their relatively smaller chords, tail rotor blades may need to be analyzed as thick-walled structures. The flex beams of bearingless main rotors are often of open cross section such as solid rectangular, I-section, or cruciform-section beams. Apart from the possibility of using different materials such as glass, graphite, and Kevlar®, various layup schemes

Received 8 May 1999; revision received 5 June 2000; accepted for publication 2 August 2001.

*Visiting Associate Professor, Alfred Gessow Rotorcraft Center, Department of Aerospace Engineering; currently Associate Professor, Research Institute of Industrial Technology, Chonbuk National University, Chonju 561-756, Republic of Korea. Member AIAA.

†Research Scientist, Alfred Gessow Rotorcraft Center, Department of Aerospace Engineering.

‡Alfred Gessow Professor and Director, Alfred Gessow Rotorcraft Center, Department of Aerospace Engineering. Fellow AIAA.

can be used for the construction of the rotor blades to improve their performance. In spite of the variety of construction features, it is possible to characterize rotor blades as thin/thick-walled beams using classical lamination theory to model the structural behavior of the skin, spars, and other load carrying members. Common to both thin-walled and thick-walled blade analysis is the need to properly model the local behavior of the shell wall in relation to the global deformation of the blade. The wall undergoes both in-plane and out-of-plane deformations (warpings) in response to applied external loading. It is important to model these warpings consistently to obtain accurate results for the beam response.[1]

To capture these nonclassical effects for a composite blade, two approaches are possible. The first class includes cross-sectional finite element analysis such as variational asymptotical beam sectional analysis (VABS)[2] that can model complex geometry and non-uniformity of a cross section. The second class, like that in the present paper, includes analytical models that are simple and can be used to provide physical insight into the relationship between the various effects. Typically, finite element models are especially useful for detailed stress analysis whereas analytical models can be useful in preliminary design and optimization studies.

The modeling of rotor blades can be formulated through either a displacement or a force method. The displacement method, also called the stiffness method, has been used by, among others, Rehfield,[3] Rehfield et al.,[4] Smith and Chopra,[5] and Chandra and Chopra.[6,7] This formulation is based on suitable approximations to the displacement field of the shell wall. The assumed displacement field is used to compute the strain energy and the beam cross-sectional stiffness relations; equations of motion are obtained through energy principles. Except for simple cross sections, there is no easy method to decide on the correct distribution of warpings. For example, torsion-related warping was assumed to be the same as that for an isotropic beam by Rehfield.[3] This was modified to include contour variation of the shear modulus by Smith and Chopra.[5] In the force method, also called the flexibility method, the assumed direct stress field in the shell wall is used to obtain the distribution of the shear stress, and the related warpings are obtained from the equilibrium equations of the shell wall. The flexibility method provides a systematic method of determining the warping functions. This method was used by Mansfield and Sobey,[8] Libove,[9] and, more recently, by Johnson et al.[10] for thin-walled composite beams with closed profiles.

Berdichevsky et al.[11] and Badir et al.[12] used the variational-asymptotic approach in which the displacement approximations were refined in an iterative manner. They applied their method to analyze thin-walled composite beams of both closed[11] and open cross sections.[12] Murakami et al.[13] proposed a Timoshenko-type beam theory based on a mixed variational principle and the use of Reissner's semicomplimentary energy function. They applied the theory to the problem of an anisotropic beam with rectangular solid cross section. The distribution of shear stresses was generated as part of the solution.

Volovoi and Hodges[14] presented an asymptotically correct, linear theory for thin-walled prismatic beams made of generally anisotropic materials. Their theory is applicable to beams of open or closed profiles and included the influence of the shell bending strain measures to obtain analytical formulas for the 4×4 cross-sectional stiffness matrix. The four strain measures used are axial, two bending, and torsion. They showed the importance of including the inplane (hoop) bending moment for a certain class of composite beams.

The present analysis uses a combination of the force and displacement methods and is a unified analysis applicable to composite blades of uniform cross section that may have open or closed profiles. The influence of thickness of the shell wall, that is, bending and shear deformations, is included in the analysis. The resulting first-order (Timoshenko) shear deformation theory describes the beam kinematics in terms of the axial, flap and lag bending, flap and lag shear, torsion, and torsion-warping deformations.

The present analysis has a number of features common with the theory of Volovoi and Hodges.[14] Both theories are applicable to composite beams with open or closed profiles and with elastic couplings. In addition, the present theory 1) includes influence of the thickness of the shell wall including shear deformation (Reissner–Mindlin) effects; 2) is a combination of the displacement and the force formulations in which the displacement formulation is used to obtain direct strains, whereas the shear related terms are obtained from the equations of equilibrium of the shell wall; 3) does not use asymptotic arguments to delete any terms; and 4) derives analytical expressions for the Timoshenko shear correction factors. The resulting first-order (Timoshenko) shear deformation theory describes the beam kinematics in terms of the axial, flap and lag bending, flap and lag shear, torsion, and torsion-warping deformations.

II. Theoretical Formulation

Figure 1a shows the geometry and generalized forces for a composite blade with an arbitrary cross section. Two systems of coordinate axes are used: an orthogonal Cartesian coordinate system, x, y, and z, for the blade, where x is the reference axis of the blade and y and z are the transverse coordinates of the cross section, and a curvilinear coordinate system, x, s, and n, for the shell wall of the section, where s is a contour coordinate measured along the middle surface of the shell wall and where n is normal to this contour coordinate. Figure 1b shows the stress resultants, moment resultants, and transverse shear forces acting on a general shell segment of the blade.

A. Kinematics

The global deformations of the beam are U, V, and W along the x, y, and z axes, and ϕ is the twist about the x axis. The local shell deformations are u, v_t, and v_n along the x, s, and n directions, respectively. When the transverse shear deformations are allowed, the local deformations at an arbitrary point on the shell wall can be expressed as

$$u = u^0 + n\psi_x, \qquad v_t = v_t^0 + n\psi_s, \qquad v_n = v_n^0 \tag{1}$$

In Eq. (1), u^0, v_t^0, and v_n^0 represent the deformations at the midplane of the shell and ψ_x, and ψ_s represent rotations of the normals to the midplane about the s and x axes, respectively. The strain–displacement and curvature–displacement relations for the wall of

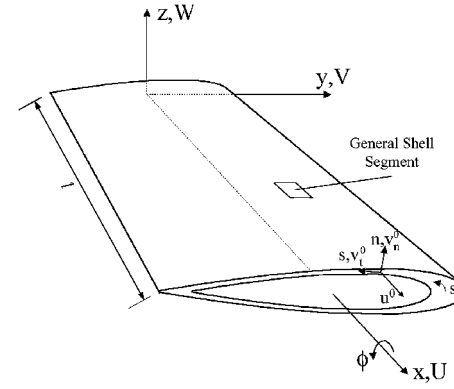

Fig. 1a Geometry and coordinate systems of a blade.

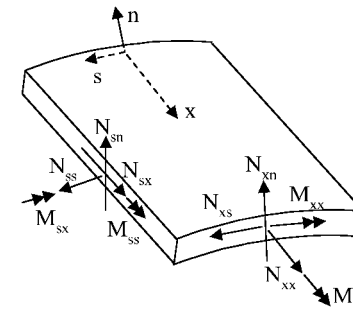

Fig. 1b Shell forces and moments.

a cylindrical shell of arbitrary geometry are given by[15]

$$\begin{Bmatrix} \varepsilon_{xx} \\ \varepsilon_{ss} \\ \gamma_{xs} \\ \gamma_{xn} \\ \gamma_{sn} \end{Bmatrix} = \begin{Bmatrix} u^0_{,x} \\ v^0_{t,s} + \left(v^0_n/a\right) \\ u^0_{,s} + v^0_{t,x} \\ v^0_{n,x} + \psi_x \\ v^0_{n,s} + \psi_s \end{Bmatrix} \tag{2a}$$

$$\begin{Bmatrix} \kappa_{xx} \\ \kappa_{ss} \\ \kappa_{xs} \end{Bmatrix} = \begin{Bmatrix} \psi_{x,x} \\ \psi_{s,s} \\ \psi_{x,s} + \psi_{s,x} \end{Bmatrix} \tag{2b}$$

In Eq. (2), a is the local shell radius of curvature. The shell midplane displacements can be obtained in terms of the beam displacements and rotations as

$$v^0_t = Vy_{,s} + Wz_{,s} + r\phi$$

$$v^0_n = Vz_{,s} - Wy_{,s} - q\phi, \qquad \psi_s = \phi \tag{3a}$$

The shell rotation and ψ_x can be obtained by equating the shear strain γ_{xn} from the beam kinematics to its value from the shell deformation:

$$\gamma_{xn} = \psi_x + v^o_{n,x} = \gamma_{xy}z_{,s} - \gamma_{xz}y_{,s}, \qquad \psi_x = \gamma_{xn} - v^0_{n,x} \tag{3b}$$

In Eq. (3b), γ_{xy} and γ_{xz} represent the shear strain of the blade and are related to β_y and β_z (the rotations of the blade cross section about the y and z axes, respectively) as

$$\beta_y = \gamma_{xz} - W_{,x}, \qquad \beta_z = \gamma_{xy} - V_{,x} \tag{4}$$

From Eqs. (1–3), the strains in the shell wall can be obtained as

$$\varepsilon_{xx} = u^0_{,x}, \qquad \gamma_{xs} = u^0_{,s} + V_{,x}y_{,s} + W_{,x}z_{,s} + r\phi_{,x}$$

$$\kappa_{xx} = \gamma_{xn,x} - v^o_{n,xx} = \beta_{z,x}z_{,s} - \beta_{y,x}y_{,s} + q\phi_{,xx}$$

$$\kappa_{xs} = \gamma_{xn,s} - v^0_{n,xs} + \phi_{,x} = 2\phi_{,x} + (1/a)(\beta_z y_{,s} + \beta_y z_{,s} - r\phi_{,x}) \tag{5}$$

In Eq. (5), the axial displacement u^0 has not yet been determined. This consists of 1) axial displacement of the beam, 2) axial warping due to bending, 3) axial warping due to torsion, and 4) axial warping due to transverse shear. To obtain a first approximation to u^0, we use the definition of shear strain. In terms of the global blade strains, the shear strain γ_{xs} is

$$\gamma_{xs} = \gamma_{xy}y_{,s} + \gamma_{xz}z_{,s} \tag{6}$$

From Eq. (2a), the shear strain is also given in terms of the displacements by

$$\gamma_{xs} = u^0_{,s} + V_{,x}y_{,s} + W_{,x}z_{,s} + r\phi_{,x} \tag{7}$$

Equating Eqs. (6) and (7) and integrating from $s = 0$ to s, we obtain the first approximation for u^0 as

$$u^0 = U + y\beta_z + z\beta_y - \bar{\omega}\phi_{,x} \tag{8}$$

where the sectorial area $\bar{\omega}$ is defined as

$$\bar{\omega} = \int_0^s r\,\mathrm{d}s \tag{8a}$$

With the relation in Eq. (8a), the strain–displacement relations in Eq. (5) can be written as

$$\varepsilon_{xx} = U_{,x} + z\beta_{y,x} + y\beta_{z,x} - \bar{\omega}\phi_{,xx}$$

$$\gamma_{xs} = u^0_{,s} + V_{,x}y_{,s} + W_{,x}z_{,s} + r\phi_{,x}$$

$$\kappa_{xx} = \beta_{z,x}z_{,s} - \beta_{y,x}y_{,s} + q\phi_{,xx}$$

$$\kappa_{xs} = 2\phi_{,x} + (1/a)(\beta_z y_{,s} + \beta_y z_{,s} - r\phi_{,x})$$

$$\gamma_{xn} = u^0_{,n} + V_{,x}z_{,s} - W_{,x}y_{,s} - q\phi_{,x} \tag{9}$$

The strain–displacement relations of Eq. (9) form the basis of the displacement method for thin/thick-walled beams.

B. Constitutive Relations

The general constitutive relations for the shell wall of the section can be written as[16]

$$\begin{Bmatrix} N_{xx} \\ N_{ss} \\ N_{xs} \\ M_{xx} \\ M_{ss} \\ M_{xs} \end{Bmatrix} = \begin{bmatrix} A_{11} & A_{12} & A_{16} & B_{11} & B_{12} & B_{16} \\ A_{12} & A_{22} & A_{26} & B_{12} & B_{22} & B_{26} \\ A_{16} & A_{26} & A_{66} & B_{16} & B_{26} & B_{66} \\ B_{11} & B_{12} & B_{16} & D_{11} & D_{12} & D_{16} \\ B_{12} & B_{22} & B_{26} & D_{12} & D_{22} & D_{26} \\ B_{16} & B_{26} & B_{66} & D_{16} & D_{26} & D_{66} \end{bmatrix} \begin{Bmatrix} \varepsilon_{xx} \\ \varepsilon_{ss} \\ \gamma_{xs} \\ \kappa_{xx} \\ \kappa_{ss} \\ \kappa_{xs} \end{Bmatrix} \tag{10a}$$

$$\begin{Bmatrix} N_{sn} \\ N_{xn} \end{Bmatrix} = \begin{bmatrix} A_{44} & A_{45} \\ A_{45} & A_{55} \end{bmatrix} \begin{Bmatrix} \gamma_{sn} \\ \gamma_{xn} \end{Bmatrix} \tag{10b}$$

where A_{ij}, B_{ij}, and D_{ij} are laminate stiffnesses for extension, extension–bending coupling, and bending, respectively. Note that, although the notations for the elastic constants in Eqs. (10a) and (10b) are those used in classical lamination theory for shells, their values depend on the initial local shell curvature. It is assumed that the hoop stress flow N_{ss} and the shear flow N_{sn} are negligibly small. In the present method, we treat the strain measures ε_{xx}, κ_{xx}, and κ_{xs} as known and derive expressions for the shear flow N_{xs} and the hoop moment M_{ss} in terms of these quantities using the equations of equilibrium of an element of the shell wall. We use the conditions that $N_{ss} = 0$ and $N_{sn} = 0$ to express ε_{ss} and γ_{sn} in terms of the other strain measures and then write Eqs. (10a) and (10b) in a semi-inverted form as

$$\begin{Bmatrix} N_{xx} \\ M_{xx} \\ M_{xs} \\ \gamma_{xs} \\ \kappa_{ss} \end{Bmatrix} = \begin{bmatrix} A_{n\varepsilon} & A_{n\kappa} & A_{n\phi} & A_{n\gamma} & A_{n\tau} \\ A_{n\kappa} & A_{m\kappa} & A_{m\phi} & A_{m\gamma} & A_{m\tau} \\ A_{n\phi} & A_{m\phi} & A_{\phi\phi} & A_{\phi\gamma} & A_{\phi\tau} \\ -A_{n\gamma} & -A_{m\gamma} & -A_{\phi\gamma} & A_{\gamma\gamma} & A_{\gamma\tau} \\ -A_{n\tau} & -A_{m\tau} & -A_{\phi\tau} & A_{\gamma\tau} & A_{\tau\tau} \end{bmatrix} \begin{Bmatrix} \varepsilon_{xx} \\ \kappa_{xx} \\ \kappa_{xs} \\ N_{xs} \\ M_{ss} \end{Bmatrix} \tag{11a}$$

$$N_{xn} = A_{xn}\gamma_{xn} \tag{11b}$$

C. Derivation of the Cross-Sectional Stiffness Relations

It is convenient to use a modified form of Reissner's semicomplimentary energy function ϕ_R (Ref. 13)

$$\begin{aligned} \Phi_R = \tfrac{1}{2}\big(&A_{n\varepsilon}\varepsilon^2_{xx} + 2A_{n\kappa}\kappa_{xx}\varepsilon_{xx} + 2A_{n\phi}\kappa_{xs}\varepsilon_{xx} + 2A_{n\gamma}N_{xs}\varepsilon_{xx} \\ &+ 2A_{n\tau}M_{ss}\varepsilon_{xx} + A_{m\kappa}\kappa^2_{xx} + 2A_{m\phi}\kappa_{xx}\kappa_{xs} + 2A_{m\gamma}\kappa_{xx}N_{xs} \\ &+ 2A_{m\tau}\kappa_{xx}M_{ss} + A_{\phi\phi}\kappa^2_{xs} + 2A_{\phi\gamma}\kappa_{xs}N_{xs} + 2A_{\phi\tau}\kappa_{xs}M_{ss} \\ &- A_{\gamma\gamma}N^2_{xs} - 2A_{\gamma\tau}N_{xs}M_{ss} - A_{\tau\tau}M^2_{ss}\big) \end{aligned} \tag{12}$$

With this definition, we have

$$\frac{\partial\Phi_R}{\partial\varepsilon_{xx}} = N_{xx}, \qquad \frac{\partial\Phi_R}{\partial\kappa_{xx}} = M_{xx}, \qquad \frac{\partial\Phi_R}{\partial\kappa_{xs}} = M_{xs}$$

$$\frac{\partial\Phi_R}{\partial\gamma_{xn}} = N_{xn}, \qquad \frac{\partial\Phi_R}{\partial N_{xs}} = -\gamma_{xs}, \qquad \frac{\partial\Phi_R}{\partial M_{ss}} = -\kappa_{ss} \tag{13}$$

To obtain the stiffness matrix relating beam forces to beam displacements we use

$$\delta\int_0^l\int_C (\Phi_R + \gamma_{xs}N_{xs} + \kappa_{ss}M_{ss})\,\mathrm{d}s\,\mathrm{d}x = 0 \tag{14}$$

where l is the length of the blade. By the use of Eqs. (2a) and (2b), Eq. (14) results in the equilibrium equations of an element of the shell wall and the constraint conditions

$$N_{xx,x} + N_{xs,s} = 0 \tag{15a}$$

$$N_{xs,x} = 0 \tag{15b}$$

$$M_{xx,x} + M_{xs,s} - N_{xn} = 0 \tag{15c}$$

$$M_{xs,x} + M_{ss,s} = 0 \tag{15d}$$

$$N_{xn,x} = 0 \tag{15e}$$

$$\gamma_{xs} - u^0_{,s} - v_{t,x} = 0 \tag{15f}$$

$$\kappa_{ss} - \psi_{s,s} = 0 \tag{15g}$$

D. Determination of N_{xs} and M_{ss}

Equation (15a) shows that N_{xs} consists of a constant part and a part that depends on the s integral of $N_{xx,x}$. Equations (15c) and (15d) show that M_{ss} has a constant part, a part that varies linearly with s, and a part that depends on the s integral of $M_{xs,x}$. Hence, we can write

$$N_{xs} = N^0_{xs} - \int_0^s (A'_{11}\varepsilon_{xx,x} + B'_{16}\kappa_{xs,x})\,\mathrm{d}s \tag{16a}$$

$$M_{ss} = M^0_{ss} + yM^y_{ss} + zM^y_{ss} - \int_0^s (B'_{16}\varepsilon_{xx,x} + D'_{16}\kappa_{xs,x})\,\mathrm{d}s \tag{16b}$$

To obtain the four unknowns N^0_{xs}, M^0_{ss}, M^y_{ss}, and M^z_{ss}, we use the following conditions of continuity of the shell wall displacements. For each cell of a closed multicell cross section[14]

$$\oint \gamma_{xs}\,\mathrm{d}s = \oint (u_{,s} + y_{,s}V_{,x} + z_{,s}W_{,x} + r_n\phi_{,x})\,\mathrm{d}s = 2A_0\phi_{,x} \tag{17a}$$

$$\oint \kappa_{ss}\,\mathrm{d}s = 0 \tag{17b}$$

$$\oint y\kappa_{ss}\,\mathrm{d}s = 0 \tag{17c}$$

$$\oint z\kappa_{ss}\,\mathrm{d}s = 0 \tag{17d}$$

If we substitute the values for γ_{xs} and κ_{ss} from Eq. (11a) into Eq. (17), we can solve for N^0_{xs}, M^0_{ss}, M^y_{ss}, and M^z_{ss}:

$$\begin{Bmatrix} N^0_{xs} \\ M^0_{ss} \\ M^y_{ss} \\ M^z_{ss} \end{Bmatrix} = [f]\{\bar{q}_b\} + [F]\{\bar{q}_b\}_{,x} \tag{18}$$

where

$$\{\bar{q}_b\}^T = \lfloor U_{,x} \quad \beta_{y,x} \quad \beta_{z,x} \quad \phi_{,x} \quad \phi_{,xx} \rfloor \tag{19}$$

With Eq. (18), the shear flow and the hoop moment, Eq. (16), can be expressed as

$$N_{xs} = N^0_{xs} + N^1_{xs}, \qquad M_{ss} = M^0_{ss} + M^1_{ss} \tag{20}$$

N^0_{xs} and M^0_{ss} depend on $\bar{q}_b$, whereas N^1_{xs} and M^1_{ss} depend on $\bar{q}_{b,x}$. Volovoi and Hodges[14] use the constraint conditions of Eq. (17) together with Lagrange multipliers in the strain energy expression. N^0_{xs}, M^0_{ss}, M^y_{ss}, and M^z_{ss} in Eq. (18) correspond to the Lagrange multipliers obtained by them. Based on asymptotic arguments, they discard $\phi_{,xx}$ for closed profiles and also discard the terms corresponding to the derivatives of $\bar{q}_b$. In Eq. (18), the first part that is dependent on the stain measures can be thought of as the active part of the shear flow. The second part is dependent on the applied forces and can be thought as the reactive shear flow.

In the present method, all of the terms are retained in Eq. (18), and Eq. (14) is used to identify the cross-sectional stress resultants as

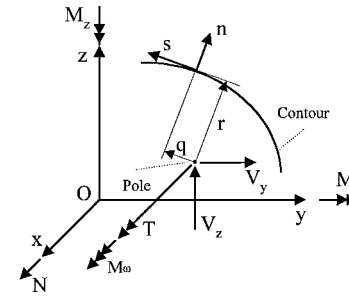

Fig. 2 Generalized beam forces and moments.

$$N = \int_C N_{xx}\,\mathrm{d}s \tag{21a}$$

$$M_y = \int_C [N_{xx}z - M_{xx}y_{,s}]\,\mathrm{d}s \tag{21b}$$

$$M_z = \int_C [N_{xx}y + M_{xx}z_{,s}]\,\mathrm{d}s \tag{21c}$$

$$M_\omega = \int_C [-N_{xx}\bar{\omega} + M_{xx}q]\,\mathrm{d}s \tag{21d}$$

$$T_s = \int_C [2M_{xs}]\,\mathrm{d}s \tag{21e}$$

$$V_y = \int_C [N_{xs}y_{,s} + N_{xn}z_{,s}]\,\mathrm{d}s \tag{21f}$$

$$V_z = \int_C [N_{xs}z_{,s} - N_{xn}y_{,s}]\,\mathrm{d}s \tag{21g}$$

where N is axial force; M_y and M_z are bending moments about the y and z directions, respectively; V_y and V_z are transverse shear forces; T_s is the St. Venant twisting moment; and M_ω is a Vlasov bimoment (Fig. 2). When Eqs. (9) and (11) are inserted into Eq. (21), the first five equations of Eq. (21) can be written as

$$\begin{Bmatrix} N \\ M_y \\ M_z \\ T \\ M_\omega \end{Bmatrix} = \{\bar{F}_b\} = [C]\{q_b\} + [D]\{q_{b,x}\} \tag{22}$$

In Eq. (22), $[C]$ is a symmetric (5×5) cross-sectional stiffness matrix and represents the idealization of the beam at an Euler–Bernoulli level for bending and Vlasov for torsion. The elements of the matrix $[D]$ are functions of the shear flow N_{xs} and the hoop moment M_{ss} and also the derivatives of the strain measures. To obtain the equivalent of a Timoshenko (first-order shear deformation) theory for the blade, we consider a cantilever blade loaded at the tip with shear forces V_y and V_z. Differentiating Eq. (22) with respect to x, we obtain

$$\{\bar{F}_{b,x}\} = \{F_s\} = \lfloor 0 \quad V_z \quad V_y \quad 0 \quad 0 \rfloor^T = [C]\{\bar{q}_{b,x}\} \tag{23}$$

or

$$\{\bar{q}_{b,x}\} = [C]^{-1}\{F_s\} \tag{24}$$

From the last two equations (21) we can obtain the force vector $\{F_s\}$ as

$$\{F_s\} = [E]\{q\} \tag{25}$$

where $\{q\}$ is the generalized displacement vector defined as

$$\{q\}^T = \lfloor U_{,x} \quad \gamma_{xy} \quad \gamma_{xz} \quad \phi_{,x} \quad \beta_{y,x} \quad \beta_{z,x} \quad \phi_{,xx} \rfloor \tag{26}$$

From Eqs. (22), (24), and (25), we obtain the 7×7 cross-sectional stiffness matrix

$$\{F\} = [\bar{K}]\{q\} \tag{27}$$

where the generalized force vector $\{F\}$ is given by

$$\{F\}^T = [N \quad V_y \quad V_z \quad T \quad M_y \quad M_z \quad M_\omega] \tag{27a}$$

The 7×7 stiffness matrix $[\bar{K}]$ of Eq. (27) represents the beam stiffness matrix at a Timoshenko level and includes the influence of the wall thickness. For thin-walled blades with closed cross sections, this stiffness matrix consists of two parts: The first is the 5×5 matrix that is equivalent to an Euler–Bernoulli approximation for bending and Vlasov for torsion, and the second part represents the correction due to the reactive shear forces.

E. Comparison with Other Theories

To compare the present theory with other formulations, we first consider the 5×5 $[\boldsymbol{C}]$ matrix in Eq. (23). This matrix is symmetric and, in general, fully populated. The beam idealization corresponds to Euler–Bernoulli for bending and Vlasov for torsion. For closed-cross-section beams, Volovoi and Hodges[14] obtain a 4×4 cross-sectional stiffness matrix, because they include only St. Venant torsion for these cross sections. Their method is similar to the present method, and the results obtained by the two methods are identical at this level of approximation. For composite beams with open cross section, Badir et al.[12] have derived similar expressions. They include terms arising from the N^0_{xs} term in Eq. (18) and neglect the correction due to N^1_{xs} using an asymptotic argument. For beams of closed cross section, Berdichevsky et al.[11] have derived the corresponding 4×4 stiffness matrix that neglected the warping restraint effects, and they do not include the thickness terms in their analysis. They also neglect the correction due to N^1_{xs} using asymptotic arguments. Given these differences, the stiffness matrices derived by Badir et al.[12] for open cross sections and Berdichevsky et al.[11] for closed cross sections are contained in the terms obtained in the present paper.

Chandra and Chopra[6,7] have extended the Vlasov theory to composite beams of both open and closed cross sections using a displacement formulation. For both types of cross sections, their model represents a Timoshenko-type theory with the shear correction factor set to unity. The stiffness matrix derived by Chandra and Chopra[7] is of the order (9×9) because they include $\gamma_{xy,x}$ and $\gamma_{xz,x}$ as independent variables in their formulation. Although these are not specifically included in the (7×7) stiffness matrix, their influence is included in the derivation of the shear flows through the use of the equilibrium equations [Eq. (15)] by eliminating $\gamma_{xs,x}$. In addition, Chandra and Chopra[7] used the zero in-plane strain assumption for the constitutive relations, whereas in the present paper the zero in-plane stress condition is used. After these factors are accounted for, the $[\bar{K}]$ matrix of the present paper agrees with that obtained by Chandra and Chopra[6,7] for both open- and closed-cross-section blades. Also, the shear related terms of the present paper agree with the corresponding terms of Ref. 6 when the shear correction factors are set to unity.

III. Finite Element Analysis

The finite element equations are derived through the application of the stationary potential energy theorem. The potential energy of the beam undergoing extension, flap and lag bending, shear, torsion, and warping deformation can be expressed as

$$\Pi = \frac{1}{2}\int_0^l \{q\}^T\{F\}\,\mathrm{d}x - \frac{1}{2}\int_0^l \{q\}^T\{f_c\}\,\mathrm{d}x \tag{28}$$

where $\{F\}$ is the generalized force vector [Eq. (27a)], $\{q\}$ is the corresponding deformations [Eq. (26)], and $\{f_c\}$ is the generalized load vector that is defined as

$$\{f_c\}^T = [n \quad q_y \quad q_z \quad t_s \quad m_y \quad m_z \quad m_\omega] \tag{29}$$

The components of $\{f_c\}$ are generalized load intensities of the beam. Inserting Eq. (27) into Eq. (28) and applying a variational statement, $\delta\Pi = 0$, yields

$$\delta\Pi = \int_0^l \{\delta q\}^T[\bar{K}]\{q\}\,\mathrm{d}x - \int_0^l \{\delta q\}^T\{f_c\}\,\mathrm{d}x = 0 \tag{30}$$

Three different types of interpolation functions are introduced to describe the behavior of the beam. For the axial displacement U, a four-node Lagrangian representation is used. The cross-sectional rotations β_y and β_z and the transverse deformations V and W are interpolated using a three-node Lagrangian shape function. For twist deformation ϕ and its derivative $\phi_{,x}$, a two-node Hermite shape function is employed to satisfy the C^1 continuity at each extremity of an element. These yield a total of 20 degrees of freedom for each finite element that can describe extension, bending, torsion, and shear deformations. Introducing this finite element representation into the energy expression [Eq. (30)], we obtain the following set of finite element beam equations:

$$[K]\{q_g\} = \{F_g\} \tag{31}$$

where $[K]$ and $\{F_g\}$ are the finite element system of stiffness matrix and load vector, respectively, and $\{q_g\}$ is the generalized displacement vector for the beam.

IV. Comparisons

Validation studies are performed by comparing the present numerical results with available experimental data and other analysis results for several different cross-sectional shapes and material distributions. The examples include single-cell box-section, I-section, and two-cell airfoil-section blades with bending–torsion and extension–torsion couplings.

A. Box Beams: 1

Volovoi and Hodges[14] presented results for the torsional stiffness of box beams with the following dimensions: outer width of 25.21 mm (0.953 in.) and outer height of 13.46 mm (0.53 in.) with a uniform wall thickness of 0.76 mm (0.03 in.). Two types of layups were considered for the walls. For the antisymmetric beam, the right and upper wall had a $[\theta_3/-\theta_3]$ layup, whereas the left and lower wall had a layup of $[-\theta_3/\theta_3]$. For the symmetric beam, the right and left walls had a $[\theta_3/-\theta_3]$ layup, whereas the upper and lower walls had a layup of $[-\theta_3/\theta_3]$. For both beams, there is very little coupling between beam bending and torsion. Each wall has a balanced layup and there is no coupling between the membrane strains ε_{xx} and γ_{xs}. An important coupling is that between the hoop moment M_{ss} and the shear strain γ_{xs}.

For the antisymmetric beam, Fig. 3 shows a comparison of the torsional stiffness obtained by different methods. The results labeled Berdichevsky et al.[11] are taken from Volovoi et al.[14] and are based on the variational asymptotic method of Ref. 11. Berdichevsky et al.[11]

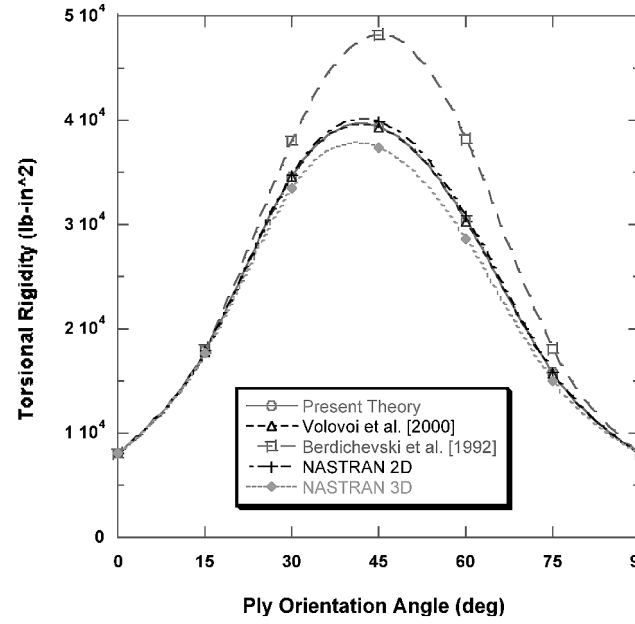

Fig. 3 Variation of torsional stiffness for a locally antisymmetric box beam with fiber layup: right and upper walls $[\theta_3/-\theta_3]$, left and lower walls $[-\theta_3/\theta_3]$.

ignored the influence of thickness for closed cross section beams based on asymptotic arguments, and the estimates obtained by this method give overestimates of the torsional stiffness. Figure 3 also shows the results obtained by the present method and by Volovoi and Hodges.[14] There is very little difference between the two sets of results. Shown in Fig. 3 are also torsional stiffnesses calculated using the MSC/NASTRAN. Results labeled 2-D NASTRAN were obtained using 360 CQUAD4 (four-noded) plate elements, and those labeled 3-D NASTRAN were obtained using 14,440 CHEXA (eight-noded) elements. It is seen that there is good agreement between all of the results.

For the symmetric beam, similar results are shown in Fig. 4. For this beam also, the results obtained by the present method agree well with those obtained by Volovoi and Hodges[14] and with the present NASTRAN results. Figure 5 shows the torsional stiffness as a function of the fiber layup angle for a locally symmetric beam with the same dimensions but with all of the walls having layups of $[\theta_3/-\theta_3]$. The results of the present method show good correlations with with the present NASTRAN results.

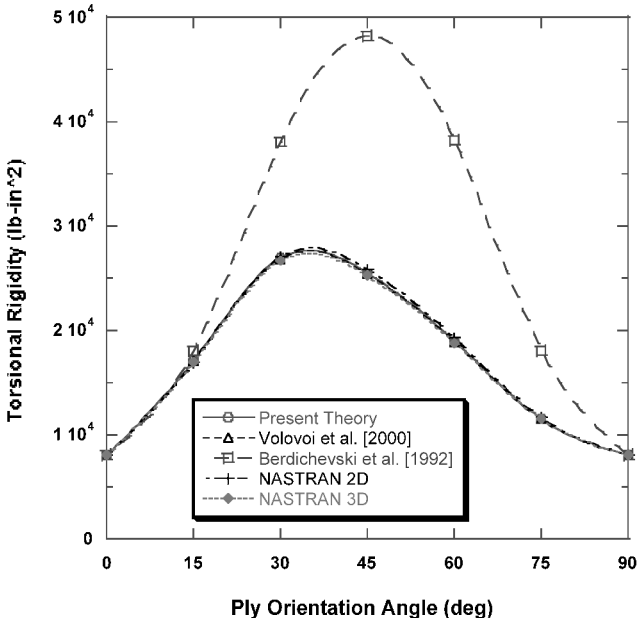

Fig. 4 Variation of torsional stiffness for a locally symmetric box beam with fiber layup: right and left walls $[\theta_3/-\theta_3]$, upper and lower walls $[-\theta_3/\theta_3]$.

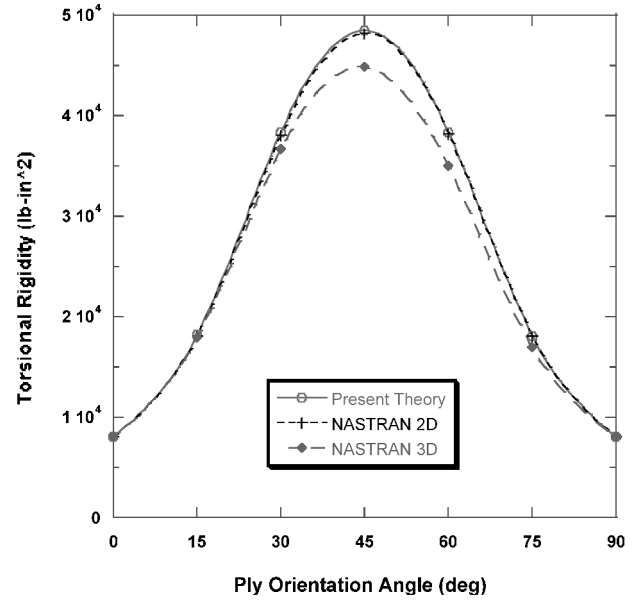

Fig. 5 Variation of torsional stiffness for a locally symmetric box beam with fiber layup: all walls $[\theta_3/-\theta_3]$.

Table 1 Geometry and material properties of AS4/3501-6 graphite–epoxy box beams (B1 and B3)

Parameter	Value
E_{11}	141.9 GPa (20.59×10^6 psi)
E_{22}	9.78 GPa (1.42×10^6 psi)
G_{12}	6.13 GPa (0.89×10^6 psi)
ν_{12}	0.42
Ply thickness	0.127 mm (0.005 in.)
Outer width	24.21 mm (0.953 in.)
Outer depth	13.64 mm (0.537 in.)
Beam length	762 mm (30 in.)

Table 2 Geometry and material properties of T300/5208 graphite–epoxy box beam (B2)

Parameter	Value
E_{11}	146.8 GPa (21.3×10^6 psi)
E_{22}	11.02 GPa (1.6×10^6 psi)
G_{12}	6.20 GPa (0.9×10^6 psi)
ν_{12}	0.42
Ply thickness	0.127 mm (0.005 in.)
Outer width	33.53 mm (1.32 in.)
Outer depth	16.76 mm (0.66 in.)

These results show that, for certain layups, it is important to include wall thickness effects in the analysis, even for beams with closed profiles.

B. Box Beams: 2

Three different composite box beams were considered. The first beam (B1) has composite ply layups of $[15]_6$ for each wall of the box section. This layup yields an antisymmetric configuration with respect to beam axis. The second beam (B2) has composite ply layups of $[(20/-70)_2/-70/20]_T$ for each wall of the box section. The beams (B1 and B2) show extension–torsion (K_{14}) and bending–shear (K_{25} and K_{36}) couplings. The third beam (B3) has symmetric (mirror image) layups of $[15]_6$ for top and bottom walls and $[15/-15]_3$ for side walls and shows bending–torsion (K_{45} and K_{46}) and extension–shear (K_{12} and K_{13}) couplings. For beams B1 and B3, the material is AS4/3501-6 graphite–epoxy, and the properties are given in Table 1. The geometry and material properties of beam B2 are given in Table 2. All of the three box beams considered are clamped at the root and free at the tip.

Table 3 shows a comparison of the nonzero stiffness coefficients obtained for the antisymmetric beam (B1) obtained from nonhomogeneous anisotropic beam section analysis (NABSA) and VABS. The NABSA and VABS results are taken from Popescu and Hodges.[17] NABSA is a detailed finite element beam model based on the work of Giavotto et al.[18] and VABS also used a detailed cross-sectional finite element analysis based on the variational asymptotic method of Cesnik and Hodges.[2] For the predictions of stiffness values with NABSA, a 216-element mesh with eight nodes per element was used, whereas VABS results were generated using 360 eight-node isoparametric elements for a total of 1200 nodes and 3600 degrees of freedom. Results using the present method were obtained in an analytic manner by evaluating cross-sectional contour integrals. The present results agree very well with those of NABSA with a maximum difference of 3.8% between the two results. The results from VABS underestimate the bending stiffnesses by 17.5 and 21.7%, respectively. The shear (both direct and coupled) stiffnesses are underestimated by between 43 and 47%. Also presented in Table 3 are results communicated by Hodges in a private communication on 2 October 2000, derived using the most recent version of VABS. These results were generated using 286 six-noded elements for a total of 672 nodes (2016 degrees of freedom). Compared with the results of Ref. 17, the results for the torsional stiffness are improved, but the large differences between the shear stiffnesses and the bending–shear coupling stiffnesses still remain. As will be shown later, these stiffnesses influence the bending displacements and are more important for beams of low slenderness ratio.

Table 3 Comparison of stiffness coefficients for the antisymmetric box beam (B1)

Stiffness	NABSA[17]	Present (%)[a]	VABS[17] (%)[a]	VABS[19] (%)[a]
$K_{11} \times 10^{7}$ (extension)	0.1438	0.1431 (0.5)	0.1445 (−0.5)	0.1432 (0.4)
$K_{14} \times 10^{6}$ (ext-torsion)	0.1075	0.1064 (1.0)	0.1090 (−1.4)	0.1060 (1.4)
$K_{22} \times 10^{5}$ (lag shear)	0.9018	0.9089 (−0.8)	0.5038 (44.0)	0.5113 (43.1)
$K_{25} \times 10^{6}$ (flap bending-lag shear)	−0.5204	−0.5391 (−3.6)	−0.2949 (43.0)	−0.2951 (43.3)
$K_{33} \times 10^{5}$ (flap shear)	0.3932	0.3822 (2.8)	0.2099 (46.0)	0.2132 (45.8)
$K_{36} \times 10^{5}$ (lag bending-flap shear)	−0.5637	−0.5605 (0.6)	−0.2984 (47.1)	−0.2989 (47.0)
$K_{44} \times 10^{5}$ (torsion)	0.1678	0.1662 (1.0)	0.1719 (−2.4)	0.1689 (−0.6)
$K_{55} \times 10^{5}$ (flap bend)	0.6622	0.6873 (−3.8)	0.5462 (17.5)	0.5513 (16.7)
$K_{66} \times 10^{6}$ (lag bend)	0.1726	0.1728 (−0.1)	0.1352 (21.7)	0.1365 (20.9)

[a]Values in parentheses denote percentage difference with respect to NABSA values and are defined as 100 × (NABSA-method)/NABSA. A positive value indicates that the method underestimates the values, and a negative value indicates an overestimate.

Table 4 Comparison of flexibility coefficients for the antisymmetric box beam (B2)

Flexibility values	NABSA	VABS	Berdichevsky et al.[11] (%)	Present (%)
$S_{\text{ext}}(S_{11} \times 10^{6})$	1.439	1.431	1.449 (+0.7)	1.443 (+0.3)
$S_{\text{ext-tor}}(S_{14} \times 10^{6})$	−4.178	−4.225	−4.301 (+2.9)	−4.269 (+2.1)
$S_{\text{tor}}(S_{44} \times 10^{5})$	3.121	3.172	3.236 (+3.6)	3.228 (+3.3)
$S_{\text{flap}}(S_{55} \times 10^{5})$	1.837	1.837	1.886 (+2.6)	1.877 (+2.1)
$S_{\text{lag}}(S_{66} \times 10^{5})$	6.143	6.194	6.345 (+3.2)	6.334 (+3.0)

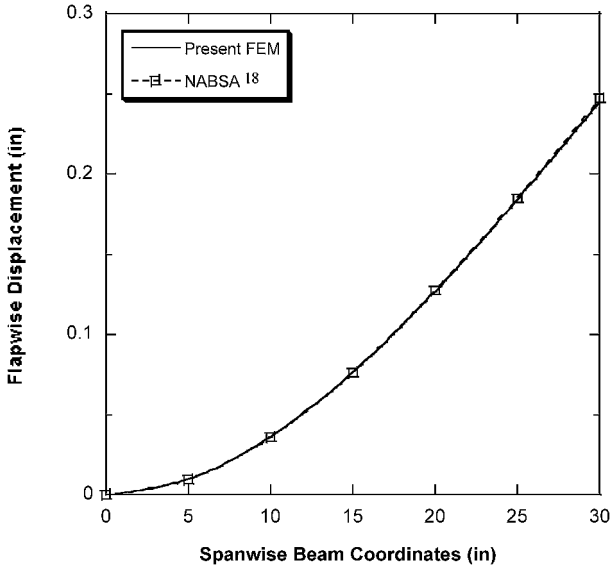

Fig. 6 Comparison of flapwise displacements for the extension-torsion coupled box beam (B1) under a unit tip bending load.

Table 4 shows a comparison of cross-sectional flexibilities for box beam B2. Also included are values from Berdichevsky et al.[11] Comparing with NABSA values, the present results in Table 4 show slightly better correlation for all of the flexibility values than those of Berdichevsky et al.[11] This is due to the inclusion of thickness effects and the terms that were neglected by Berdichevsky et al.[11] This correlation in sectional properties of beam B2 resulted in the excellent agreement between the present beam results and those of NABSA for the flapwise static beam deflections, as shown in Fig. 6. The two predictions are almost identical.

The variation of twist angle along the length of the extension-torsion coupled beam (B1) that is subjected to unit tip torque is shown in Fig. 7. Experimental data from Chandra and Chopra[20] are presented for comparison. Six beam finite elements were used for the present calculation. The correlation between the present approach with the experimental results is shown to be good. Figures 8 and 9 show the comparison of results for the bending slope variation and the bending induced twist distribution along the beam span for the symmetric layup box beam (B3) under a unit tip bending load.

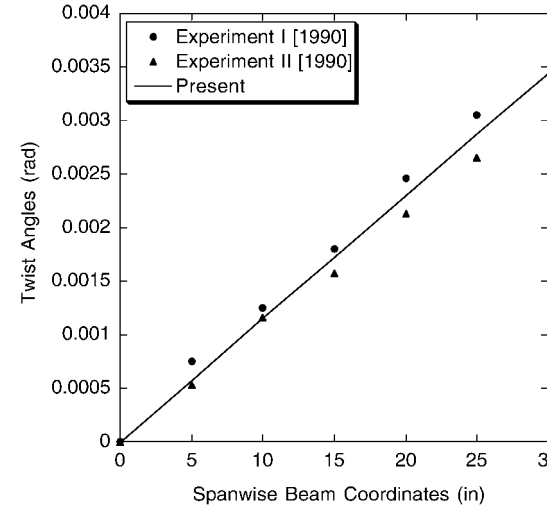

Fig. 7 Comparison of twist distribution for the extension–torsion coupled box beam (B1) under a unit tip torque.

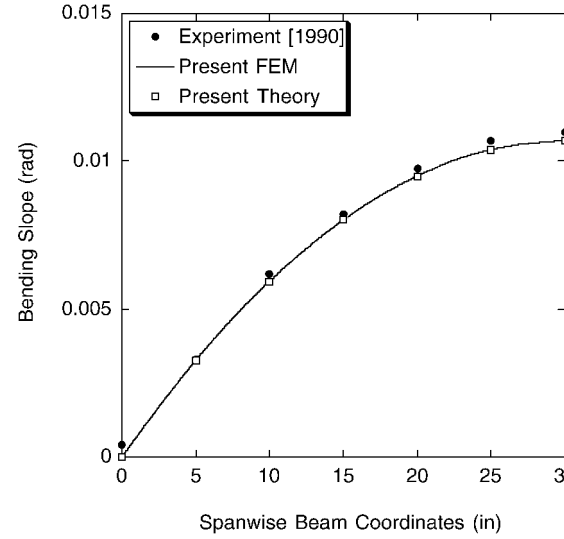

Fig. 8 Comparison of bending slope for the bending–torsion coupled box beam (B3) under a unit tip bending load.

This beam has bending–torsion and extension–shear couplings. Experimental data from Chandra and Chopra[19] are also presented. The results of a closed-form solution similar to Ref. 20 are also shown in Figs. 8 and 9; these show good correlation with the present finite element results. In general, the predictions of the present analysis are in good agreement with experimental results. Disparity of correlation for the induced twist distribution (Fig. 9) near the beam tip may be due to boundary constraints imposed on the tested beams.

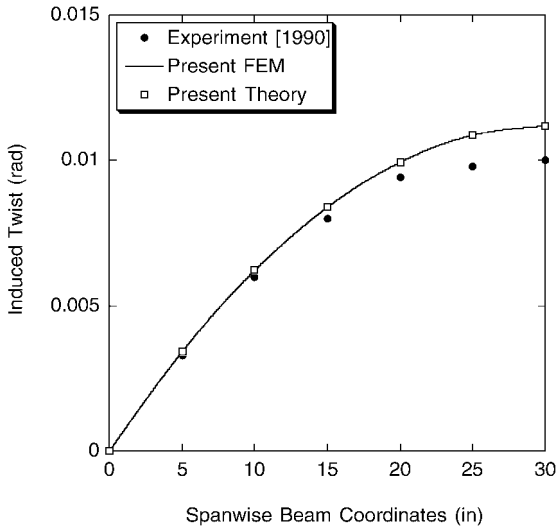

Fig. 9 Comparison of twist distribution for the bending–torsion coupled box beam (B3) under a unit tip torque.

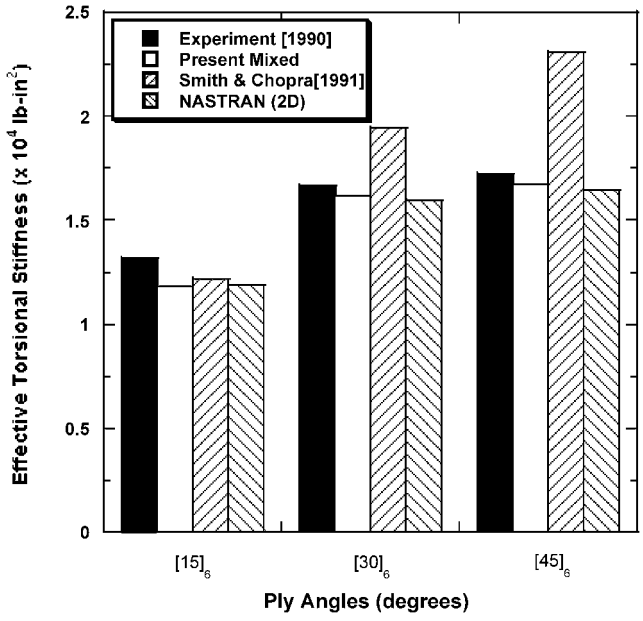

Fig. 10 Comparison of effective torsional stiffness for bending–torsion coupled box beams.

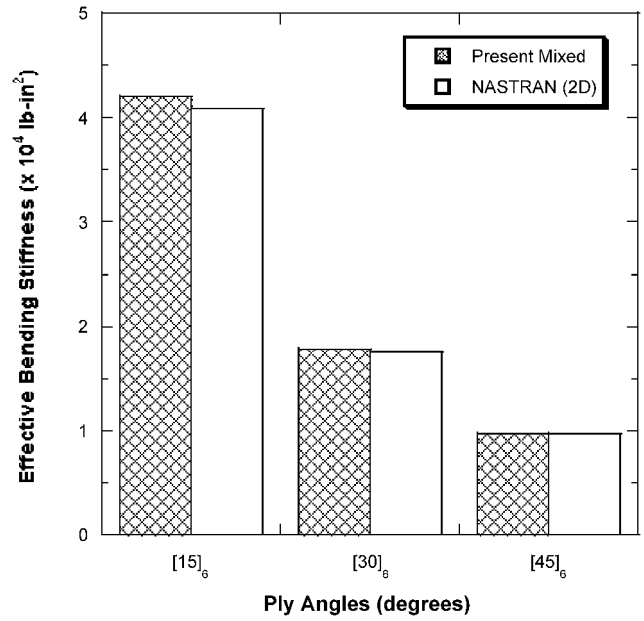

Fig. 11 Comparison of effective bending stiffness for bending–torsion coupled box beams

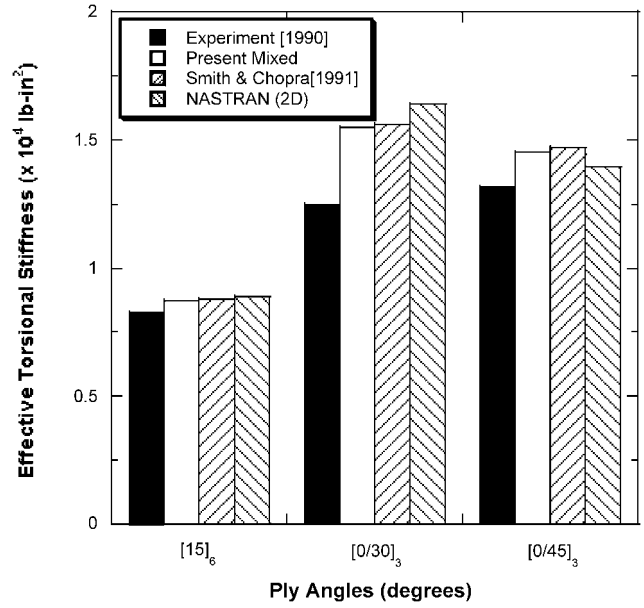

Fig. 12 Comparison of effective bending stiffness for extension–torsion coupled box beams

Figures 10 and 11 show comparisons of the effective torsional and bending stiffnesses for bending–torsion coupled beams similar to blade B3 for three fiber angles. Shown are the results derived from experiment,[19] Smith and Chopra,[5] the present method, and values calculated using MSC/NASTRAN two-dimensional plate elements. To generate the finite element results, 720 elements with 745 nodes and 3531 degrees of freedom were used. Figures 12 and 13 show similar comparisons for the effective bending and torsional stiffnesses for extension–torsion coupled box beams similar to beam B1. The results from the present method agree well with NASTRAN results.

C. I Beam

The I beams tested by Chandra and Chopra[6] are used for validation studies. The material properties of these beams are given in Table 1. The beam has a length of 762 mm (30 in.) with a 25.4×12.7 mm (1×0.5 in.) section. The beam is clamped at its root and warping restrained at both the root and loading tip. The fabrication techniques and testing procedures are described in detail in Ref. 6. Figure 14 shows the layup configuration for the bending–torsion coupled I beams. The I section has a symmetric layup with respect to beam elastic axis and is composed of top and bottom flanges with a layup of $[(0/90)_2/(90/0)/15_2]_T$ and a web with $[0/90]_{2s}$.

Figure 15 presents the bending slope distribution along the beam span for the bending–torsion coupled I beam under a unit tip bending load using the present mixed method and the stiffness method. The displacement method used to calculate the stiffnesses follows Smith and Chopra,[5] but it uses the constitutive relations given by Eq. (11). As can be seen in Fig. 15, the current predictions with mixed formulation show better correlation with experimental data. The stiffness-based approach underestimates bending slope of the beam. Figure 16 presents the bending-induced twist distribution along the beam span for the same beam under a unit tip bending load. It is surprising that the stiffness method shows better correlation with the test data than the mixed method. The warping restraint imposed at the beam tip in analysis may be too restrictive and result in an overestimate of the torsional stiffness of the beam. Figure 17 shows the twist distribution along the beam subjected to unit tip torque. The present results of using a mixed formulation show a somewhat better correlation with experimental results. This is due to the higher accuracy in estimating bending, warping, and torsion stiffnesses in the present mixed formulation. Again, the overall estimations are

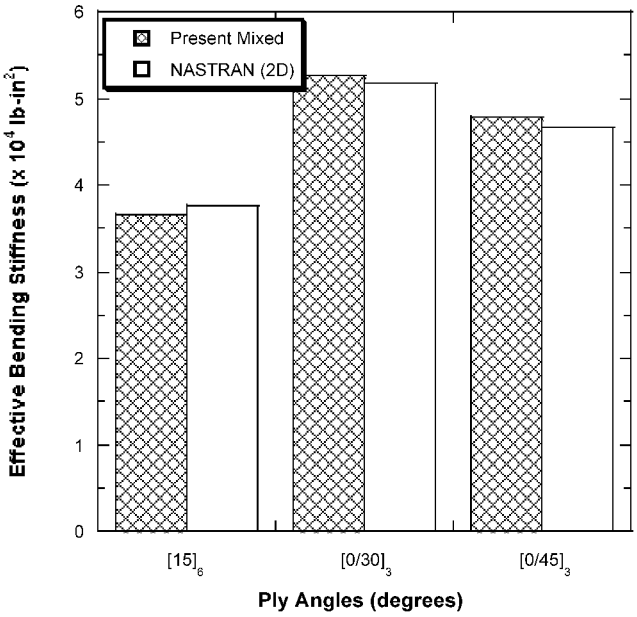

Fig. 13 Comparison of effective torsional stiffness for extension–torsion coupled box beams

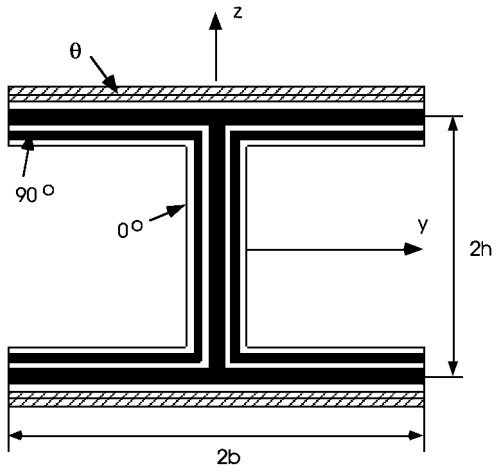

Fig. 14 Layup configuration for a bending–torsion coupled I beam; flanges $[(0/90)_2/(90/0)/\theta_2]_T$ and web $[(0/90)_2]_s$.

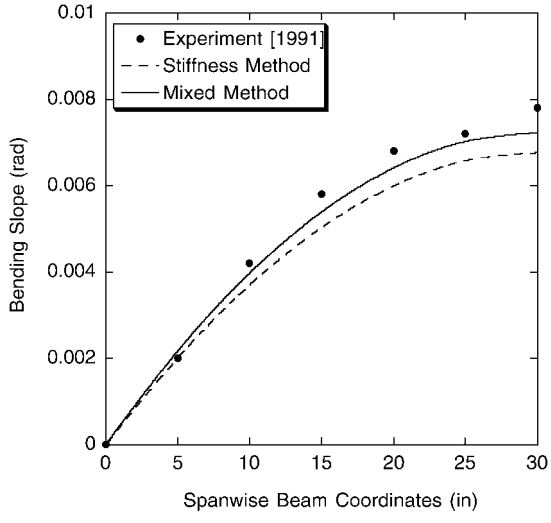

Fig. 15 Comparison of bending slope for the bending–torsion coupled I beam under a unit tip bending load; flanges $[(0/90)_2/(90/0)/15_2]_T$ and web $[(0/90)_2]_s$.

poor near the beam tip, and this may be a result of imposed warping restraint there.

D. Two-Cell Blades

Figure 18 shows the cross section of the two-cell blade tested by Chandra and Chopra.[20] The blade is clamped at one end and warping restrained at both ends ($\phi'|_{x=0} = \phi'|_{x=l} = 0$). The geometry of the blade and the mechanical material properties are given in Table 5. The airfoil blade section consists of both D spar and web with a layup of $[0/\theta]_3$ and skin with layup of $[\theta/-\theta]$. The composite ply orientation angle is varied from 0 to 90 deg.

Figure 19 shows the comparison results of the tip bending slope as a function of ply orientation angle under unit tip bending load.

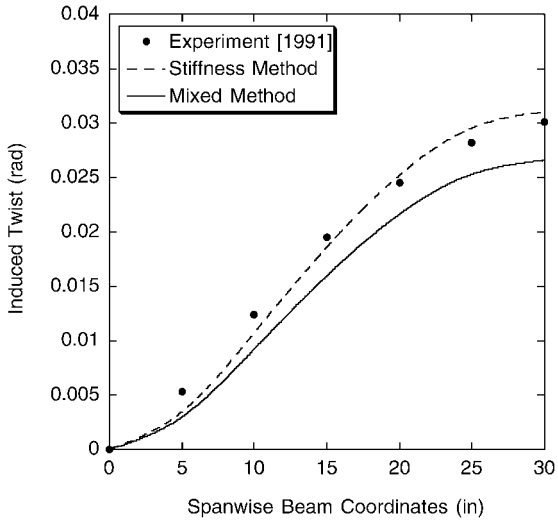

Fig. 16 Comparison of bending-induced twist distribution for the bending–torsion coupled I beam under a unit tip bending load; flanges $[(0/90)_2/(90/0)/15_2]_T$ and web $[(0/90)_2]_s$.

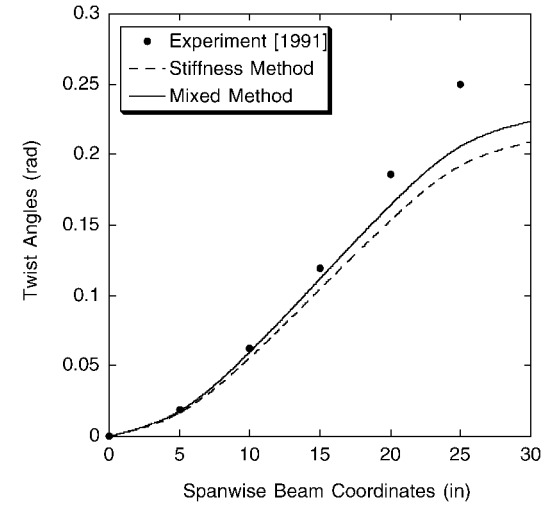

Fig. 17 Comparison of twist distribution for the bending–torsion coupled I beam under a unit tip torque; flanges $[(0/90)_2/(90/0)/15_2]_T$ and web $[(0/90)_2]_s$.

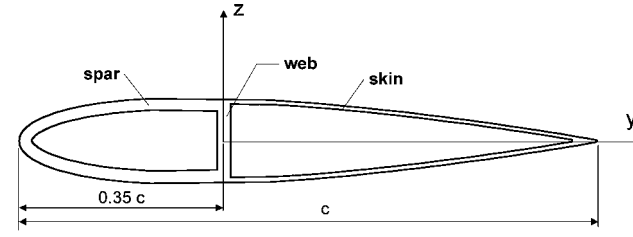

Fig. 18 Schematic of two-cell blade section.

Table 5 Geometry and material properties of a graphite–epoxy composite blade

Parameter	Value
E_{11}	131 GPa (19×10^6 psi)
E_{22}	9.3 GPa (1.35×10^6 psi)
G_{12}	5.86 GPa (0.85×10^6 psi)
ν_{12}	0.40
Ply thickness	0.127 mm (0.005 in.)
Airfoil	NACA 0012
Length	711.2 mm (28 in.)
Chord	76.2 mm (3 in.)
Airfoil thickness	9.144 mm (0.36 in.)

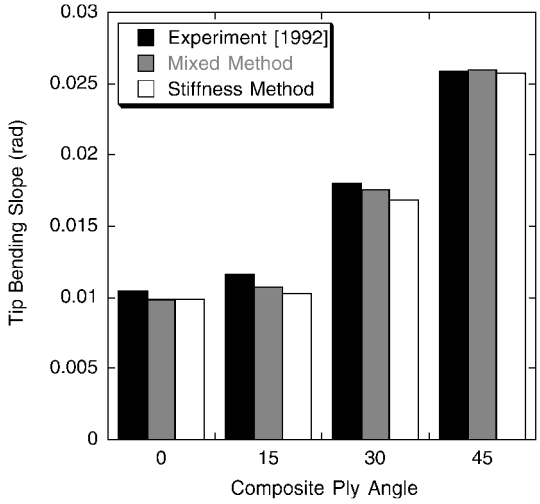

Fig. 19 Comparison of tip bending slope for extension–torsion coupled blades under a unit tip bending load.

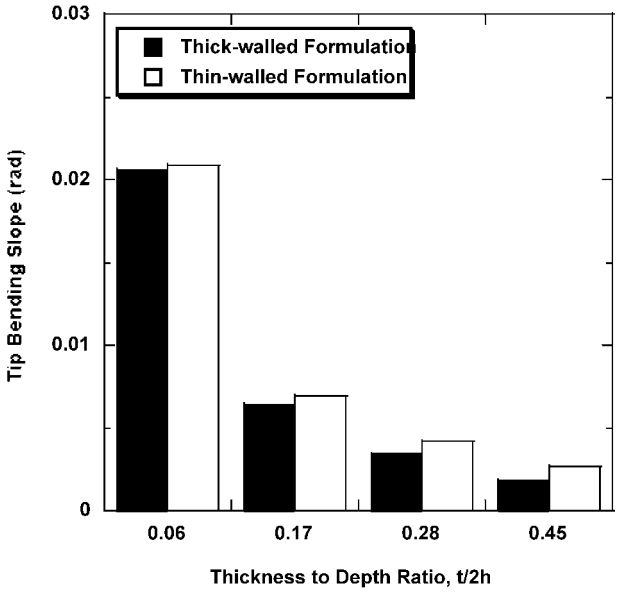

Fig. 20 Effects of wall thickness on the tip bending slope for bending–torsion coupled box beams under a unit tip bending load.

The present results with mixed formulation are seen to give better correlation with experimental results compared with those obtained from the stiffness formulation. The correlation between analysis and experiments is within 5%. The influence of the layup on the bending flexibility is substantial, namely, about a 250% increase in bending slope at the tip compared to the baseline uncoupled layup.

E. Thickness Effect

Figures 20 and 21 show the influence of wall thickness on the bending and twist deformations, respectively, for bending–torsion

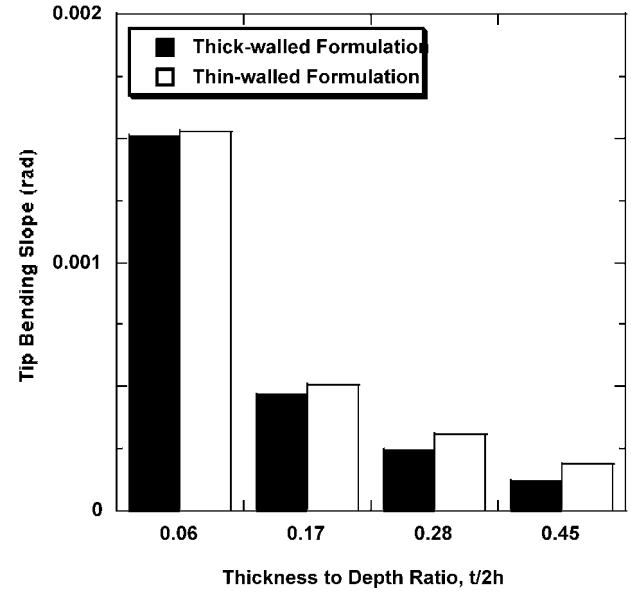

Fig. 21 Effects of wall thickness on the tip twist for bending–torsion coupled box beams under a unit tip torque.

coupled composite box beams under unit tip bending load. The results obtained by using both thick-walled and thin-walled approximations are presented. In the thin-walled formulation, the membrane assumption is used for the shell wall, whereas in the thick-walled formulation, the bending behavior of the shell wall is also included. For this configuration, the layup for top and bottom flanges of the box beam is $[30]_{6n}$, and that for side flanges is $[30/-30]_{3n}$. The layer parameter n is varied as 1, 3, 5, and 8. When the layer parameter reaches 8, the total number of layers is 48. At this layer number, the thickness-to-depthratio of the section becomes 0.45. The thickness-to-depth ratio of the box section is defined as the ratio of the wall thickness divided by the outer depth of the section ($t/2h$). As can be seen in figs. 20 and 21, wall thickness effects become larger as the wall thickness increases, and the errors due to neglect of wall thickness effects become significant when the thickness-to-depth ratio passes at or above 0.2. At this ratio, the error is around 10%. As expected, the assumption of a thin wall underestimates stiffnesses. Note that the error is larger for the twist response (Fig. 21) than for the bending response (Fig. 20). This is due to the dominant role of $A_{\phi\phi}$ in the torsional stiffness (C_{55}), which is varied as a function of cubic of wall thickness, whereas in the bending stiffness (C_{22} or C_{33}), the primary component is $A_{n\varepsilon}$, and this is varied as a function of wall thickness itself. The induced beam response due to the elastic coupling of composites is similar to the direct beam response and is not presented.

F. Transverse Shear Effect

The influence of transverse shear deformation is twofold: the direct transverse shear effect and transverse-shear-relatedcoupling effect. The direct transverse shear effect is controlled both by the slendernessratio of the beam and its cross-sectionaldetails, whereas the effect of transverse-shear-related couplings is controlled by only the cross-sectional details.

Figure 22 shows the influence of the bending–shear coupling on the predicted flapwise tip displacement of extension–torsion coupled composite box beams under unit tip bending load. For the calculation, each of the four walls of the box section has a layup of $[0/\theta]_3$ and the ply angle θ is varied from 0 to 90 deg. The bending–shear coupling has a negligible influence on the bending behavior for this specific beam with a slenderness ratio of 56. The effect of layup angle change on the transverse shear behavior of this beam is shown to be insignificant. In Fig. 23, the percentage error in the flapwise tip displacement as a result of neglecting the effect of transverse shear for beam B1 ($[15]_6$) is plotted as a function of the slenderness ratio of the box beam. The percentage error is defined as $|W_{\text{tip}} - W^0_{\text{tip}}|/W_{\text{tip}} \times 100$, where W_{tip} and W^0_{tip} are flapwise tip displacements

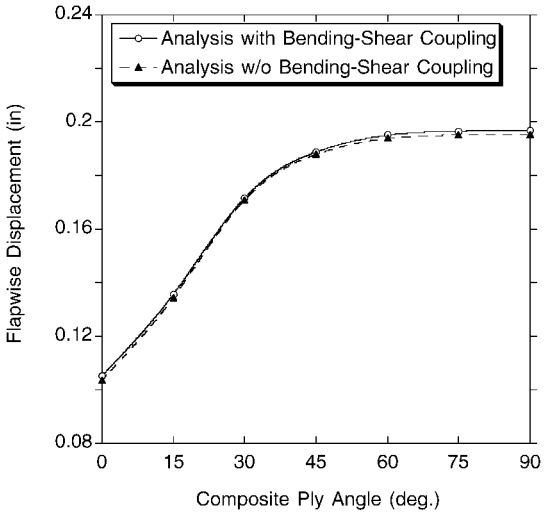

Fig. 22 Effects of transverse shear on the flapwise tip displacement of extension–torsion coupled box beams; $[0/\theta]_3$ and $l/2h = 56$.

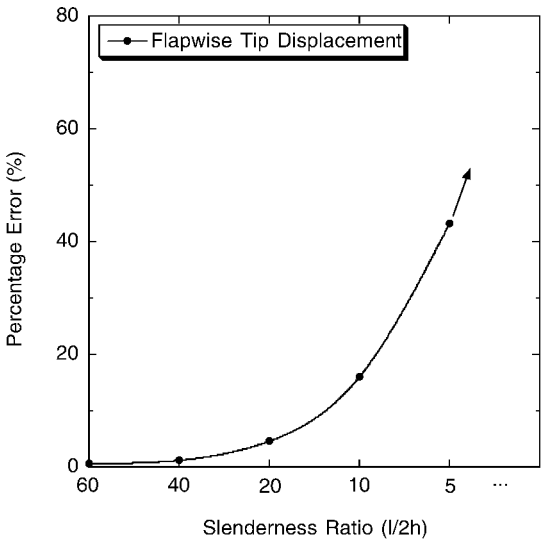

Fig. 23 Percentage error in flapwise tip displacement due to the neglect of transverse shear for the extension–torsion coupled box beam (B1).

obtained with and without transverse-shear couplings, respectively. As is shown in Fig. 16, the slenderness ratio has a significant influence on the bending behavior of the beam. For beams with a slenderness ratio of 20, the percentage error between the two predictions is less than 5%, whereas for beams with a slenderness ratio of 5, this value becomes as high as 43%. Figure 24 shows the influence of bending–shear coupling on the flapwise tip displacement of composite I beams under unit tip bending load. The I beam has layup of top and bottom flanges with $[(0/90)_2/(90/0)/\theta_2]_T$ and web with $[(0/90)_2]s$. The slenderness ratio of the beam is 56. The effects of bending–shear couplings on the bending response of I beams are more significant than those of box beams, as can be seen in this plot: For beams with a 15-deg layup, the percentage error is 3.1%. This is due to thicker walls used in the I section than in the box section. Again, the change of ply angle on the transverse shear behavior of the beam is small. Figure 25 shows the percentage error in flapwise tip displacement calculated with and without bending–shear couplings for the open-section I beam with a flange layup of $[(0/90)_2/(90/0)/15_2]_T$. Again, the slenderness ratio of the beam has a large effect on the prediction of beam bending response. For the I beam with slenderness ratio of 20, the error due to neglecting the bending–shear couplings is within 8%. However, when the slenderness ratio of the beam is five, the error exceeds 60%.

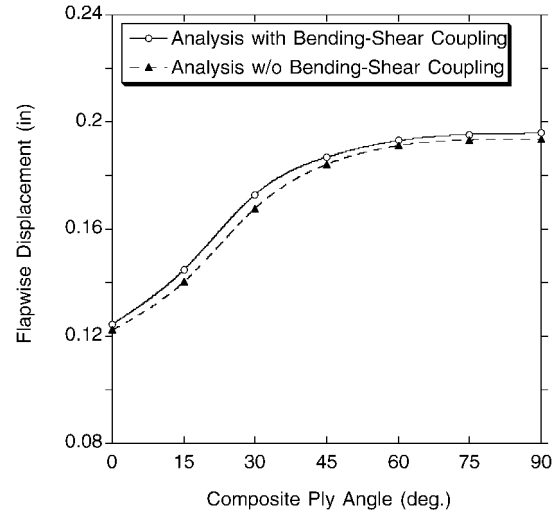

Fig. 24 Effects of transverse shear on the flapwise tip displacement of extension–torsion coupled I beams; flanges $[(0/90)_2/(90/0)/\theta_2]_T$ and web $[(0/90)_2]_s$, $l/2h = 56$.

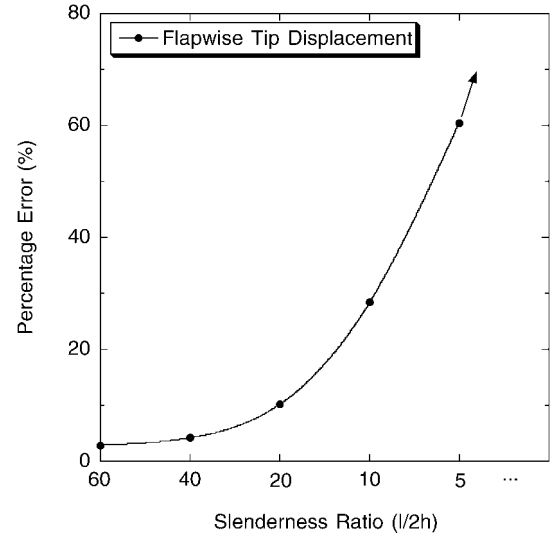

Fig. 25 Percentage error in flapwise tip displacement due to the neglect of transverse shear for the extension–torsion coupled I beam; flanges $[(0/90)_2/(90/0)/15_2]_T$ and web $[(0/90)_2]_s$.

V. Summary

A refined structural model applicable to both thick- and thin-walled composite blades, which can have either an open or closed profile with either a single- or multiple-cell section, has been developed. The model includes the influence of the thickness of the shell wall and accounts for the nonuniform distribution of the shear strains across the section. Extensive validation studies have been performed to correlate the present results against experimental test data and other detailed finite element results for graphite-epoxy composite beams of various cross sections such as I sections, box sections, and two-cell airfoil sections. Plate and three-dimensional elements of MSC/NASTRAN were used for some specific beams to generate additional results. Good correlations were achieved for all of the bending–torsion and extension–torsion coupled beams and blades.

For certain layups, it is important to include the influence of wall bending stiffeness in the analysis and to consider wall thickness. The wall thickness effects are shown to become significant when the thickness-to-depth ratio of the beam reaches around 20%. At this ratio, the error is around 10%. It is shown that the thickness effect on the twist response is more pronounced than for the bending response.

The transverse shear deformation is shown to influence the structural behavior of the coupled beams in terms of the slenderness

ratio and layup configuration of the beam. The slenderness ratio has a significant effect on the transverse shear behavior of the beam. The effects are larger for beams with low slenderness ratios. For beams with a slenderness ratio of 20, the error due to the neglect of transverse shear is less than 5% for the box beam and less than 8% for the open-section I beam, whereas for beams with a slenderness ratio of 5, the errors become 43% for the box beam and exceed 60% for the I beam. It is shown that the layup angle has a nonnegligible effect on the transverse shear behavior of the beam.

Acknowledgments

This work was supported by the National Rotorcraft Technology Center under Grant NCC 2944. The Technical Monitor is Yung Yu. We acknowledge the contribution of graduate students Kyung-Min Dong and Jong-Duck Park, Department of Aerospace Engineering, Chonbuk National University, Republic of Korea, in providing the two- and three-dimensional and NASTRAN analysis results. We thank and acknowledge the many thoughtful comments and discussions with Dewey Hodges of the Georgia Institute of Technology.

References

[1]Jung, S. N., Nagaraj, V. T., and Chopra, I., "Assessment of Composite Rotor Blade Modeling Techniques," *Journal of the American Helicopter Society*, Vol. 44, No. 3, 1999, pp. 188–205.

[2]Cesnik, C. E. S., and Hodges, D. H., "VABS: A New Concept for Composite Rotor Blade Cross-Sectional Modeling," *Journal of the American Helicopter Society*, Vol. 42, No. 1, 1997, pp. 27–38.

[3]Rehfield, L. W., "Design Analysis Methodology for Composite Rotor Blades," Seventh DOD/NASA Conf. on Fibrous Composites in Structural Design, AFWAL-TR-85-3094, Denver, CO, June 1985, pp. V̇(a)1–V̇(a)5.

[4]Rehfield, L. W., Atilgan, A. R., and Hodges, D. H., "Nonclassical Behavior of Thin-Walled Composite Beams with Closed Cross Sections," *Journal of the American Helicopter Society*, Vol. 35, No. 2, 1990, pp. 42–51.

[5]Smith, E. C., and Chopra, I., "Formulation and Evaluation of an Analytical Model for Composite Box-Beams," *Journal of the American Helicopter Society*, Vol. 36, No. 3, 1991, pp. 23–35.

[6]Chandra, R., and Chopra, I., "Experimental and Theoretical Analysis of Composite I Beams with Elastic Couplings," *AIAA Journal*, Vol. 29, No. 12, 1991, pp. 2197–2206.

[7]Chandra, R., and Chopra, I., "Structural Response of Composite Beams and Blades with Elastic Couplings," *Composites Engineering*, Vol. 2, Nos. 5–7, 1992, pp. 347–374.

[8]Mansfield, E. H., and Sobey, A. J., "The Fiber Composite Helicopter Blade, Part I: Stiffness Properties, Part II: Prospects for Aeroelastic Tailoring," *Aeronautical Quarterly*, Vol. 30, Pt. 2, May 1979, pp. 413–449.

[9]Libove, C., "Stress and Rate of Twist in Single-Cell Thin-Walled Beams with Anisotropic Walls," *AIAA Journal*, Vol. 26, No. 9, 1988, pp. 1107–1118.

[10]Johnson, E. R., Vasiliev, V. V., and Vasiliev, D. V., "Anisotropic Thin-Walled Beams with Closed Cross-Sectional Contours," *Proceedings of the AIAA/ASME/ASCE/AHS/ASC 39th Structures, Structural Dynamics, and Materials Conference*, AIAA, Reston, VA, 1998, pp. 500–508.

[11]Berdichevsky, V. L., Armanios, E., and Badir, A., "Theory of Anisotropic Thin-Walled Closed-Cross-Section Beams," *Composites Engineering*, Vol. 2, Nos. 5–7, 1992, pp. 411–432.

[12]Badir, A. M., Berdichevsky, V. L., and Armanios, E. A., "Theory of Composite Thin-Walled Opened-Cross-Section Beams," *Proceedings of the AIAA/ASME/ASCE/AHS/ASC 34th Structures, Structural Dynamics, and Materials Conference*, AIAA, Washington, DC, 1993, pp. 2761–2770.

[13]Murakami, H., Reissner, E., and Yamakawa, J., "Anisotropic Beam Theories with Shear Deformation," *Journal of Applied Mechanics*, Vol. 63, No. 3, 1996, pp. 660–668.

[14]Volovoi, V. V., and Hodges, D. H., "Theory of Anisotropic Thin-Walled Beams," *Journal of Applied Mechanics*, Vol. 67, No. 3, 2000, pp. 453–459.

[15]Kraus, H., *Thin Elastic Shells*, Wiley, New York, 1967, p. 200.

[16]Jones, R. M., *Mechanics of Composite Materials*, 2nd ed., Taylor and Francis, 1999, pp. 195–198.

[17]Popescu, B., and Hodges, D. H., "On Asymptotically Correct Timoshenko-Like Anisotropic Beam Theory," *International Journal of Solids and Structures*, Vol. 37, No. 3, 2000, pp. 535–558.

[18]Giavotto, V., Borri, M., Mantegazza, P., Ghiringhelli, G., Carmaschi, V., Maffioli, G. C., and Mussi, F., "Anisotropic Beam Theory and Applications," *Computers and Structures*, Vol. 16, Nos. 1–4, 1983, pp. 403–413.

[19]Chandra, R., and Chopra, I., "Thin-Walled Composite Beams Under Bending, Torsional, and Extensional Loads," *Journal of Aircraft*, Vol. 27, No. 7, 1990, pp. 619–626.

[20]Chandra, R., and Chopra, I., "Structural Behavior of Two-Cell Composite Rotor Blades with Elastic Couplings," *AIAA Journal*, Vol. 30, No. 12, 1992, pp. 2914–2921.

E. Raymond
Associate Editor